Journal of Alloys and Compounds 509 (2011) 8554–8560

Contents lists available at ScienceDirect

Journal of Alloys and Compounds

journal homepage: www.elsevier.com/locate/jallcom

Development of high strength Sn–0.7Cu solders with the addition of small amount of Ag and In

A.A. El-Daly*, A.E. Hammad

Physics Department, Faculty of Science, Zagazig University, Zagazig, Egypt

ARTICLE INFO

Article history:
Received 4 April 2011
Received in revised form 29 May 2011
Accepted 31 May 2011
Available online 8 July 2011

PACS:
62.20.Fe
61.82.Bg
61.66.Dk

Keywords:
Lead-free solder
Sn–Cu alloy
Microstructure
Intermetallic compounds
Tensile properties

ABSTRACT

Nowadays, a major concern of Sn–Cu based solder alloys is focused on continuously improving the comprehensive properties of solder joints formed between the solders and substrates. In this study, the influence of Ag and/or In doping on the microstructures and tensile properties of eutectic Sn–0.7Cu lead free solder alloy have been investigated. Also, the effects of temperature and strain rate on the mechanical performance of Sn–0.7Cu, Sn–0.7Cu–2Ag, Sn–0.7Cu–2In and Sn–0.7Cu–2Ag–2In solders were investigated. The tensile tests showed that while the ultimate tensile strength (UTS) and yield stress (YS) increased with increasing strain rate, they decreased with increasing temperature, showing strong strain rate and temperature dependence. The results also revealed that with the addition of Ag and In into Sn–0.7Cu, significant improvement in YS (~255%) and UTS (~215%) is realized when compared with the other commercially available Sn–0.7 wt. % Cu solder alloys. Furthermore, the Sn–0.7Cu–2Ag–2In solder material developed here also exhibits higher ductility and well-behaved mechanical performance than that of eutectic Sn–0.7Cu commercial solder. Microstructural analysis revealed that the origin of change in mechanical properties is attributed to smaller β-Sn dendrite grain dimensions and formation of new inter-metallic compounds (IMCs) in the ternary and quaternary alloys.

1. Introduction

Traditional Sn–Pb solders have long been considered as the most popular materials for electronic packaging, since they have a low melting point, low cost and good wettability [1]. Despite all of these advantages, a rapid switching to Pb-free solders has occurred to replace the toxic Pb-based solders in the packaging process of electronic devices and components. Indeed, many research groups have been focused on developing new Pb-free solders [2,3]. But new solders must fulfill several requirements such as; low material cost, good wettability, suitable melting temperature, excellent mechanical and electrical properties, high corrosion resistance and acceptability for health and environment [4]. Previously, several types of binary and ternary Sn-based lead-free solders such as; Sn–Zn, Sn–Ag, Sn–Cu, Sn–Ag–Zn and Sn–Ag–Cu have been developed and applied in the electronic packaging industry [5,6]. The most promising Pb-free alternative appears to be the Sn–Cu eutectic or near eutectic alloy system, which has already been introduced into industrial production due to their superior properties such as; low-cost, prohibiting dissolution of Cu substrate and availability, especially for iron, dip and wave soldering operations [7]. The melting point of eutectic composition is relatively high (227 °C) when compared to the Sn–Pb (183 °C) [8]. Nevertheless, there has been only a limited amount of data about the mechanical properties of Sn–Cu solder and its joint [9,10].

However, the mechanical strength of Sn–0.7Cu synthesized using equilibrium solidification processes is relatively low when compared to the Sn–Pb or Sn–Ag–Cu system, and this may lead to reliability issue. In addition, the solderability of Sn–0.7Cu solder was poorer than that of Sn–Pb, Sn–Ag and Sn–Ag–Cu eutectic solders [11]. Also, the tensile and shear strength of Sn–Cu eutectic solder were found to be inferior to those of Sn–Ag and Sn–Ag–Cu eutectic solders. Interestingly, it was also found that the Sn–Cu eutectic alloy has substandard mechanical properties when compared with other lead-free solders and even with Pb–Sn solders [10]. On the other hand, the Sn–Cu Pb-free solder joints typically have a bad solder joint appearance, insufficient oxidation resistance characteristic that can be more of issues for wave soldering applications [12]. Thus, it is expected to improve its mechanical properties and oxidation resistance performance by adding trace amount of elements such as; Ag [10,11], P [11] and Mo [13]. Chuang et al. [14] showed that by adding Ag into the Sn–Cu system, the melting temperature can be reduced from 227 °C to 217 °C, which reduces the magnitude of thermal stresses during soldering and improves the solder reliability. In addition, the high Ag content and strong Cu_6Sn_5 phases of a well designed Sn–Ag–Cu alloy solder can promote

* Corresponding author. Tel.: +20 552325030; fax: +20 552308213.
E-mail address: dreldaly11@yahoo.com (A.A. El-Daly).

0925-8388/$ – see front matter © 2011 Elsevier B.V. All rights reserved.
doi:10.1016/j.jallcom.2011.05.119

Table 1
Chemical composition of the solders studied (wt.%).

Alloy	Cu	Ag	In	Pb	Bi	Sb	As	Sn
Sn–0.7Cu	0.7	–	–	0.012	0.007	0.011	0.006	Bal.
Sn–0.7Cu–2Ag	0.7	2	–	0.014	0.009	0.016	0.008	Bal.
Sn–0.7Cu–2In	0.7	–	2	0.014	0.010	0.019	0.009	Bal.
Sn–0.7Cu–2Ag–2In	0.7	2	2	0.014	0.009	0.016	0.008	Bal.

enhanced joint strength and creep resistance [10]. Li et al. [11] also showed that the trace P addition into Sn–Cu alloy can increase the rate of forming void of Sn–0.7Cu solder joint, which can potentially enhance crack initiation in the solder joint. Hodulova et al. observed that a small amount of Ni addition to lead-free solders produced more of the Cu_6Sn_5 phase during the reflow stage [9]. It was therefore suggested that this thicker Cu_6Sn_5 phase becomes a better diffusion barrier for the Sn atomic flux necessary for the Cu_3Sn growth. On the other hand, Zeng et al. [12] showed that the major benefits of rare earth element Pr on Sn–Cu–Ni lead-free solder are improving the solderability, refining the microstructure, and depressing the IMC growth. However, extensive experimental investigations have also been conducted on the mechanical properties of bulk solder alloys, and various testing methods have been used for investigating the mechanical properties of lead-free solder balls [15].

Since the selection of materials for solder alloys is critical and plays an important role in solder joint reliability [16], the present work is devoted to investigate the effects of small amount of Ag and/or In additions on the microstructure and tensile properties of Sn–Cu eutectic solder alloy. Also, the effects of temperature and strain rate on the mechanical properties of all solder alloys were investigated. The relationship between microstructure and mechanical properties was discussed.

2. Experimental procedures

Pure tin (99.999 pct), silver (99.999 pct), copper (99.99 pct), and indium (99.999 pct) were used as raw materials and melted in a vacuum furnace at 600 °C for 2 h to produce solder alloys of Sn–0.7Cu (SC), Sn–0.7Cu–2Ag (SC–Ag), Sn–Cu–2In (SC–In) and Sn–0.7Cu–2Ag–2In (SC–AgIn) alloys (all in wt.%). The molten solders in crucible were homogenized and then poured chill cast in a steel mold to form cylindrical ingots of 10 mm in diameter. A cooling rate of 6–8 °C/s was achieved, so as to create the fine microstructure typically found in small solder joints in microelectronic packages [17]. Chemical compositions of the solder alloys are listed in Table 1. For investigation the microstructure, the specimens were mechanically polished with 0.5 μm Al_2O_3 particles and etched with 2% HCl, 3% HNO_3 and 95% (vol.%) C_2H_5OH solution. Examination was carried out by a JEOL scanning electron microscope (SEM). Phase identification of the alloy samples were carried out by X-ray diffractometry (XRD) at 40 kV and 20 mA using Cu K_α radiation with diffraction angle (2θ) from 25° to 85° and a constant scanning speed of 1° min^{-1}. The solder ingots were then mechanically machined into a wire samples. Tensile specimens have a gauge section of 3.5×10^{-2} m in length and 2.5×10^{-3} m in diameter. All specimens were heat-treated at 130 °C for 30 min to remove the residual stress and defects induced during preparation [10]. Tensile tests were carried out with (Instron 3360 Universal Testing Machine) at constant strain rate of 1.2×10^{-2} s^{-1} and different temperatures in the range from 25 to 110 °C. The tests also were conducted at 70 °C using strain rates ranging from10^{-3} to 10^{-2} s^{-1} to determine the effect of Ag and In contents on the mechanical properties of mixed alloy as well as to determine the effect of strain rate on strength. Each datum represents an average of three measurements. The environment chamber temperature could be monitored by using a thermocouple contacting with specimen.

3. Results and discussion

3.1. X-ray diffraction analysis

X-ray diffraction (XRD) was carried out at all the as-solidified SC, SC–Ag, SC–In and SC–AgIn samples (see Fig. 1). Only body-centered tetragonal (bct) β-Sn and Cu_6Sn_5 IMC phases were detected in all the SC-based samples. XRD analysis confirmed that the Sn and Cu display successful alloying of Sn and Cu after the solidified process. The addition of Ag into the SC solder alloy can result in formation of new Ag_3Sn IMC phase due to alloying of Sn and Ag (Fig. 1(b)). Also, Fig. 1(c) shows the presence of γ-$InSn_4$ phase due to alloying of Sn and In with SC–In alloy sample. In the case of SC–AgIn, it is seen that the microstructure consisted of three new IMCs phases, i.e. Ag_3Sn, In_4Ag_9 and γ-$InSn_4$ (Fig. 1(d)).

3.2. Microstructures of as-solidified solder alloys

Fig. 2(a–d) shows the typical microstructure of as-solidified solder alloys. In Fig. 2(a), a coarse microstructure of SC alloy was formed, which consisted of Sn colonies and eutectic network with spherical Cu_6Sn_5 IMC particles of 0.5 μm. In addition, some of the particles build thin "walls" around small β-Sn areas. These walls are often one or more particles thick. However, some large particles of Cu_6Sn_5 were also identified in Fig. 2(a). With the addition of 2 wt.% Ag, the solidified microstructure exhibits eutectic network with Cu_6Sn_5 and Ag_3Sn IMC particles in the Sn matrix of SC–Ag

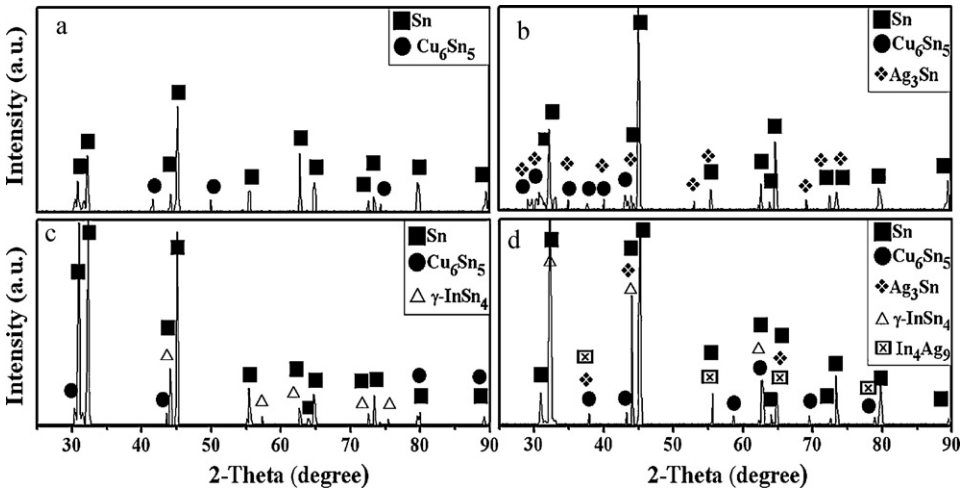

Fig. 1. XRD patterns of (a) Sn–0.7Cu, (b) Sn–0.7Cu–2Ag, (c) Sn–0.7Cu–2In and (d) Sn–0.7Cu–2Ag–2In solder alloys.

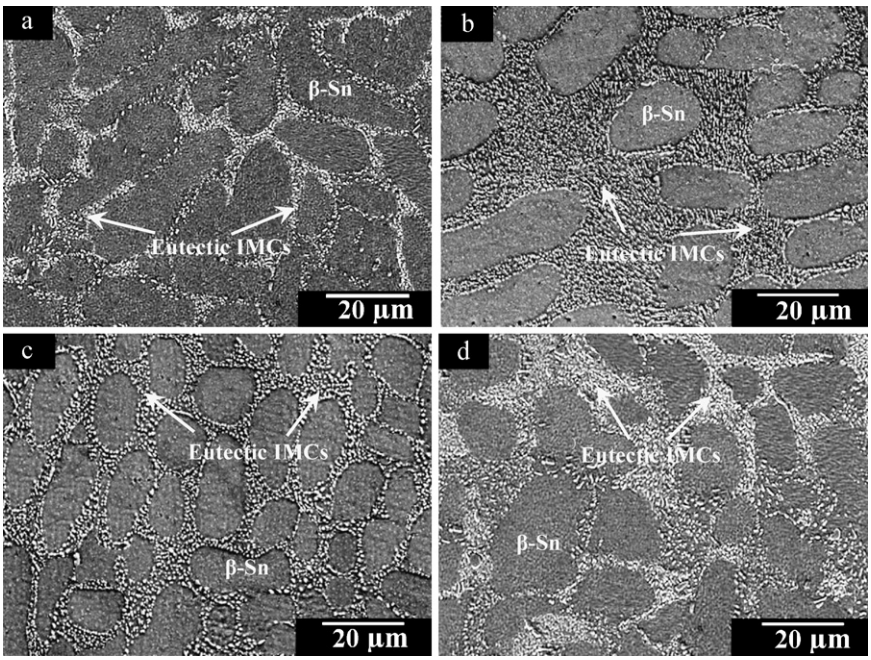

Fig. 2. Microstructures of as-solidified (a) Sn–0.7Cu, (b) Sn–0.7Cu–2Ag, (c) Sn–0.7Cu–2In and (d) Sn–0.7Cu–2Ag–2In solder alloys.

alloy. The width of the eutectic colonies turns to be much thicker than the SC solder. Since the Ag has little solubility in β-Sn near room temperature (0.004 wt.% [18]), which was expected to be fine nuclei for solidification, the fine Ag_3Sn and Cu_6Sn_5 IMC particles are refined and evenly distributed in the β-Sn matrix, rather than forming bigger rod-shape precipitates in the solder matrix, as shown in Fig. 2(b). With the addition of In into the SC alloy, clusters of fine γ-$InSn_4$ and Cu_6Sn_5 IMC sphere particles are surrounded by particle free β-Sn areas. The eutectic network and β-Sn phases in the SC-In solder become more refined and well ordered (see Fig. 2(c)). In the microstructure of SC–AgIn specimens, the fine Ag_3Sn, Cu_6Sn_5, In_4Ag_9 and γ-$InSn_4$ IMC particles are formed and arranged in densely packed areas, as shown in Fig. 2(d). These areas are interrupted by relatively small β-Sn phases (mean diameter approximately 20 μm). From these results, we anticipated that the microstructural change would affect the mechanical properties of the solder alloy.

3.3. Tensile tests

The experimental results of mechanical tests of SC, SC–Ag, SC–In and SC–AgIn samples are shown in Fig. 3. The comparison of tensile stress–strain curves was performed at constant strain rate of $1.2 \times 10^{-2}\ s^{-1}$ at room temperature. The results reveal that strain hardening instead of strain softening has occurred for all specimens, which can be ascribed to the strengthening mechanism of IMC phases in the alloy matrix. These results are consistent with our previous work [8]. However, during strain hardening, the dislocation density increases with intensifying the deformation leading to further hindering of the dislocation movement. As the dislocation density increases and the resistance to their motion increases, the imposed stress that is necessary to deform the material increases with increasing strain hardening [19]. Consequently, the formation of new IMCs in the ternary and quaternary solder alloys initiates the UTS and YS in these alloys. The average values of UTS, YS and elongations of the studied alloys are given in Fig. 4 and listed in Table 2. The SC–AgIn alloy shows the highest tensile strength among the four solders investigated. The UTS of the as-solidified SC–AgIn, which has the value of 47.3 MPa, is approximately 1.7, 1.3 and 1.2 times that of SC, SC–In and SC–Ag alloys, respectively. Also, for the same

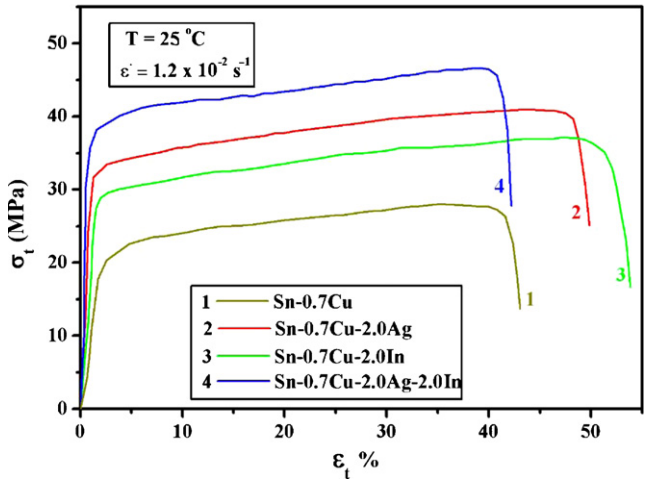

Fig. 3. Comparative tensile stress–strain curves obtained at $T = 25\ ^\circ C$ and $\dot{\varepsilon} = 1.2 \times 10^{-2}\ s^{-1}$ for Sn–0.7Cu, Sn–0.7Cu–2Ag, Sn–0.7Cu–2In and Sn–0.7Cu–2Ag–2In solder alloys.

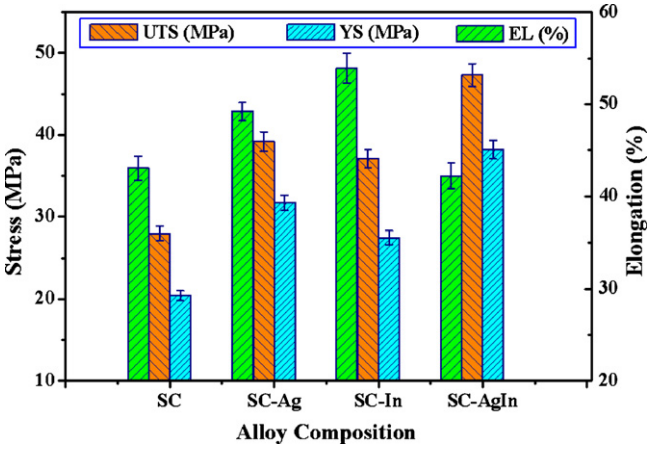

Fig. 4. Mechanical properties of the samples: tensile strength and elongation (UTS: ultimate tensile strength; YS: yield strength; EL: total elongation).

Table 2
Tensile properties of Sn–0.7Cu, Sn–0.7Cu–2Ag, Sn–0.7Cu–2In and Sn–0.7Cu–2Ag–2In solder alloys at $T = 25\,^{\circ}C$ and $\dot{\varepsilon} = 1.2 \times 10^{-2}\ s^{-1}$.

Alloy	UTS (MPa)	YS (MPa)	Elongation (%)
Sn–0.7Cu	28.0	20.4	44.0
Sn–0.7Cu–2Ag	39.2	31.6	49.2
Sn–0.7Cu–2In	37.1	28.8	53.9
Sn–0.7Cu–2Ag–2In	47.3	38.2	42.2
Sn–0.7Cu [20]	22.0	15.0	39.0
Sn–3.5Ag [20]	26.7	22.5	24.0
Sn–37Pb [20]	31.0	27.0	48.0

strain rate, the YS of SC–AgIn alloy is the highest one, which has the value of 38.2 MPa, being 1.9 times that of SC alloy and 1.3 times that of SC–In as well as 1.2 times that of SC–Ag alloys. Because of the presence of different IMCs in the SC–AgIn alloy, confirmed by XRD analysis (Fig. 1), the highest UTS and YS values are properly consistent with the previous findings [8]. However, these strength values are still higher than that of the widely used commercial solders [20], as seen in Table 2. By comparing SC–AgIn solder developed in this study with the eutectic Sn–0.7 wt.% Cu [20], the YS increased by ~255%, while UTS increased by ~215%.

The elongations to failure for SC, SC–Ag, SC–In and SC–AgIn solder alloys were 44.0, 49.2, 53.9 and 42.2%, respectively. The obtained data are comparable with those found in the literatures for Sn–0.7Cu, SAC and Sn–0.3Ag–0.7Cu–2.0In alloy values [6,21,22].

3.4. Fracture surfaces of alloy samples

Fig. 5 shows the fracture morphology of SC, SC–Ag, SC–In and SC–AgIn solder alloys after tensile tests. In general, typical dimple fracture surfaces were observed for each specimen, which indicate that the fracture type of all the solder alloys was ductile fracture. However, the fracture morphology of the four solder samples displays different characteristics. In Fig. 5(a), the fracture surface of the SC solder alloy consists of relatively large ductile-dimples and some fine IMCs were observed in the surface. In case of SC–Ag solder, the fracture surface exhibits small dimples appearance and characteristic of obvious plastic deformation. The sizes of these dimples were much smaller than that of SC solder. It can be clearly seen that the fracture is almost occurred in the bulk solder (Fig. 5(b)). Likewise, in Fig. 5(c), the SC–In solder appeared to behave similarly with SC–Ag solder, but the micro-voids formed during fracture process were larger in scale than that of SC–Ag solder, and the fracture surface had occurred near the interface of solder joint. Conversely, for SC–AgIn solder, the fracture surface was a mixture of fine ductile-dimples and a few large voids (Fig. 5(d)). The dimple was relatively larger than that of SC–Ag and SC–In solders. As we can see, the morphology of fracture surface is consistent with the results of tensile tests.

3.5. Effect of strain rate on the mechanical properties of solders

Fig. 6 shows the effect of strain rate on UTS, YS and total elongations of the four solder alloys at 70 °C. All alloys demonstrated an increase in both UTS and YS with increasing strain rate. Such behavior comes from the interaction between IMCs or precipitates with the dislocation motion. At low strain rates, the precipitates hinder the fast moving dislocation. With increasing strain rate, the IMCs cannot capture the moving dislocation any more due to the faster velocity of the dislocation in the alloy. Therefore, when the stress is applied to the solder, the dislocations slip on the slip planes which can tolerate the deformation. Since the β-Sn-rich phase is the basic microstructure of the SC-based solders, the IMCs between Sn, Ag and In such as; Ag_3Sn, Cu_6Sn_5, γ-$InSn_4$ and In_4Ag_9 make the solder exhibits high strength. The IMCs also produce smaller dendrites Sn-rich phase, which lead to an improvement in the tensile strength. For that reasons, the SC–AgIn demonstrated the highest UTS and YS values when compared to the other studied alloys, whereas a substantial improvement in UTS and YS also are observed for the separate addition of Ag and In into the Sn–Cu binary alloy. These results for SC and SC–Ag are consistent with the testing results given by Zeng et al. [10]. On the other hand, the plastic flow is directly related to the increase of strain rate, except at strain rate of $1.0 \times 10^{-3}\ s^{-1}$. It seems that the non-uniform cast structure of the samples could have possibly affected the UTS, YS and elongation. On the microscale, material structure is piecewise discontinuous and heterogeneous owing to the existence of micro-defects or damage. Based on the equivalence principle [35], the micro-defects can be

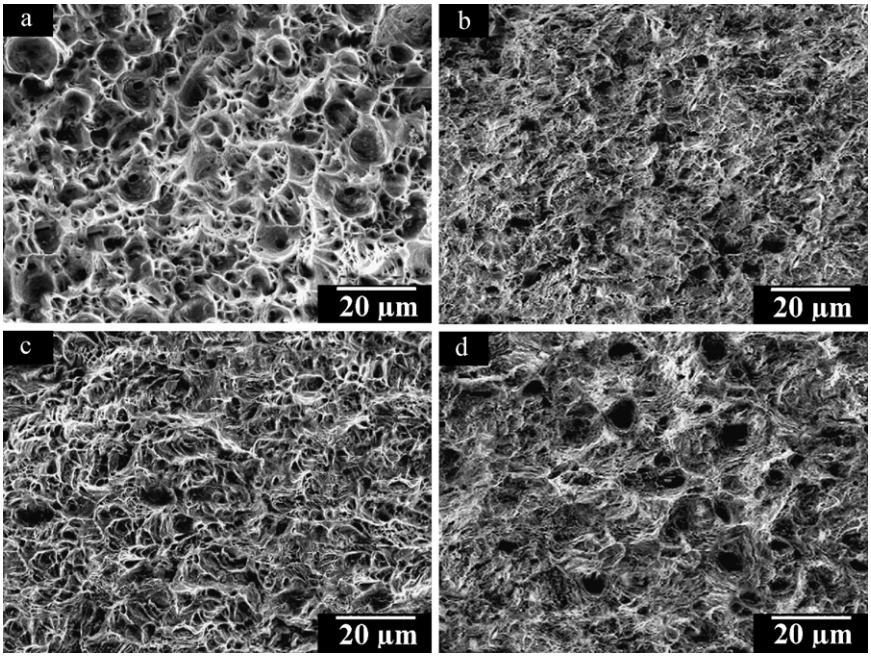

Fig. 5. SEM fractrograph for (a) Sn–0.7Cu, (b) Sn–0.7Cu–2Ag, (c) Sn–0.7Cu–2In and (d) Sn–0.7Cu–2Ag–2In solder alloys.

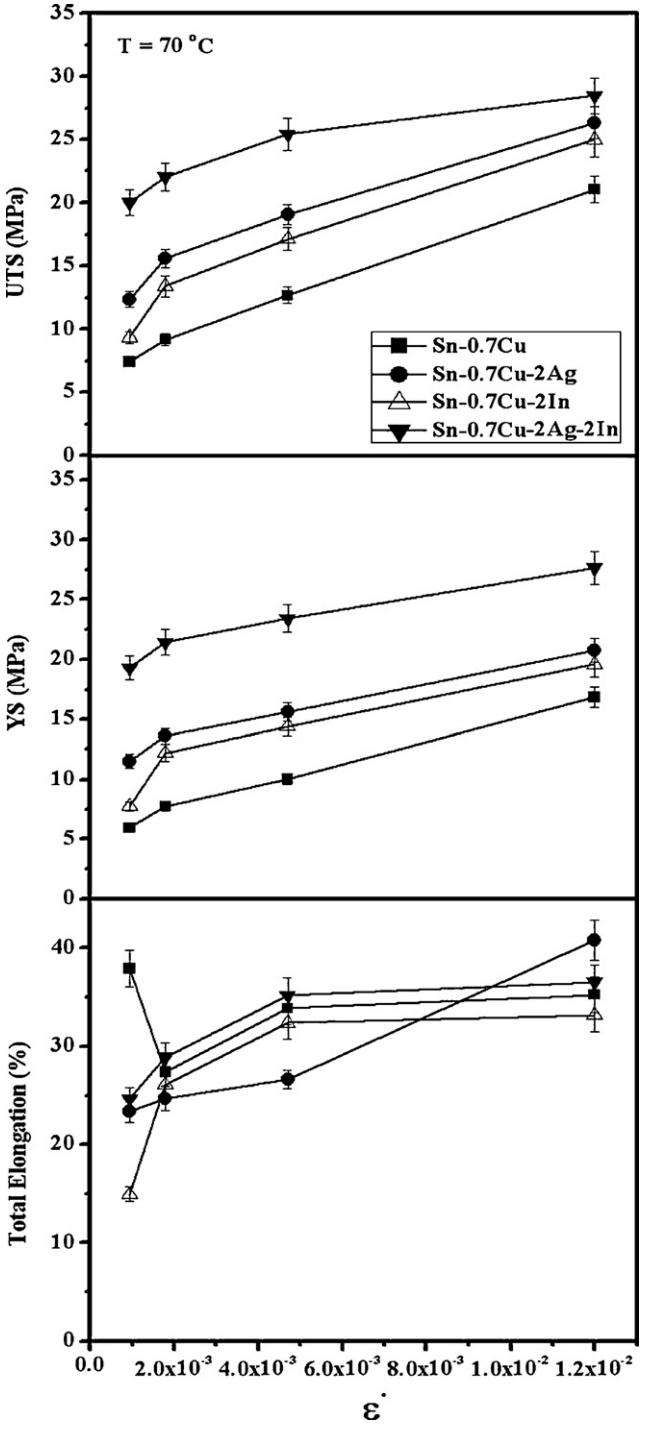

Fig. 6. Effect of strain rate on: ultimate tensile strength (UTS), yield stress (YS) and total elongation for Sn–0.7Cu, Sn–0.7Cu–2Ag, Sn–0.7Cu–2In and Sn–0.7Cu–2Ag–2In solder alloys at 70 °C.

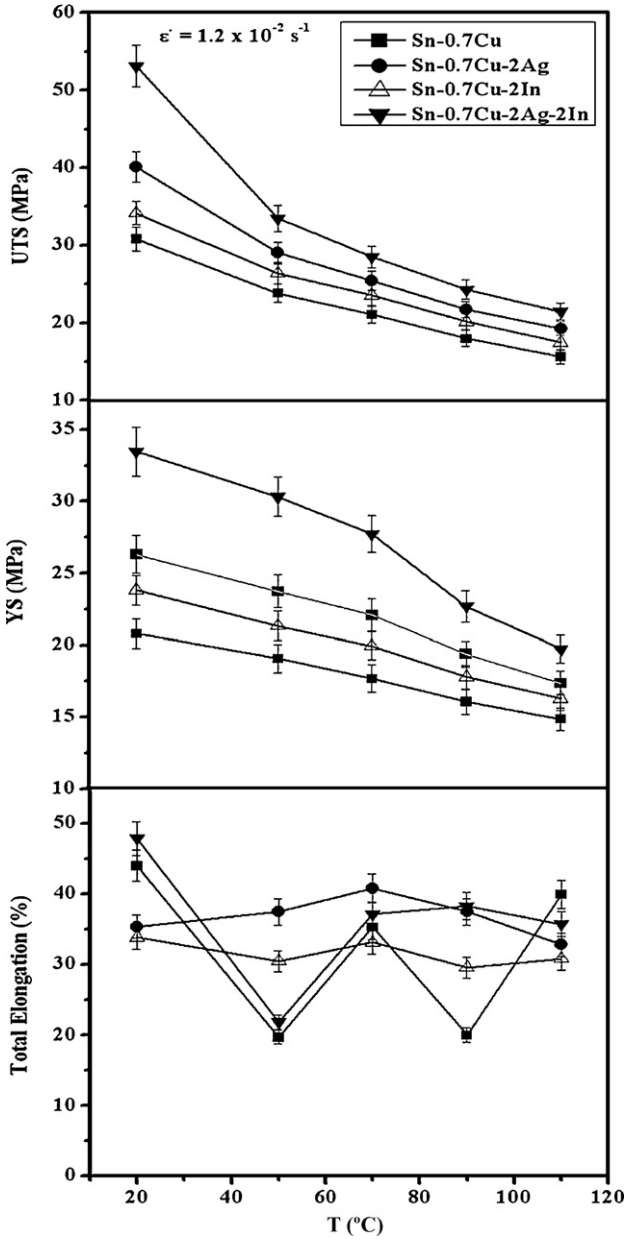

Fig. 7. Effect of temperature on; ultimate tensile strength (UTS), yield stress (YS) and total elongation for Sn–0.7Cu, Sn–0.7Cu–2Ag, Sn–0.7Cu–2In and Sn–0.7Cu–2Ag–2In solder alloys at strain rate of $1.2 \times 10^{-2}\ s^{-1}$.

'smeared out' and the stress and strain state can be considered as homogeneous. However, no attempt is made to identify the physical nature of the damage parameters and to distinguish between different damage mechanisms.

3.6. Effect of temperature on the mechanical properties of solders

In addition to the importance of deformation resistance of Pb-free solder alloys, the mechanical behavior at different temperatures and constant strain rate of these solders was also defined a very crucial thermomechanical property. Fig. 7 shows the effect of testing temperature on the UTS, YS and the total elongations of the solder alloys at strain rate of $1.2 \times 10^{-2}\ s^{-1}$. It is noted that with increasing temperature, the UTS and YS were decreased. Similar behavior was observed by other researchers working on SAC and SC solders [22,23]. Besides, with increasing testing temperature, the dynamic recovery of lead-free solder becomes dominant in the process of tensile deformation, which results in decreasing the stress levels of UTS and YS. Therefore, the solder becomes more ductile and subtle when testing temperature increases. However, Fig. 6 also reveals that, at all the examined temperatures, the Sn–0.7Cu–2Ag–2In alloy has the highest tensile strength values. In contrast, the Sn–Cu alloy exhibits the lowest one. Nevertheless, the ductility as measured by percent elongation has decreased and increased with inconsistent behaviors. Consistently with the present study, it was reported that at high homologous tempera-

tures, the elongation of ductile materials does not always increase or decrease with either increasing temperature or decreasing strain rate, and the best ductility is usually obtained at certain temperature and strain rate [24]. However, to understand this phenomenon more clearly, it is required to study the physical properties of each IMC further. The further development was made by Ashby and Edward [25,26] to analyze the creep damage and failure of different materials. It is believed that the deterioration of high temperature material results from different mechanisms, e.g. grain boundary sliding, ductile void growth, diffusion of vacancies along the boundary and IMC precipitate coarsening, etc. To take into consideration of the effects of these different damage mechanisms on creep failure, multi-variable constitutive equations were thus developed. Conversely, several possible explanations can exist for the sensitivity of ductility to testing temperatures. These include compositional and heat treatment effects on the matrix phase and IMC chemistries, impurity segregation to interfaces, the nature of interface formed between the IMCs and the matrix, the growth rate and stability of the soft and hard IMCs in the alloy matrix, the change of strain rate sensitivity or stress exponent with temperature [17].

3.7. Stress exponent

The stress exponent (n) and activation energy (Q) are two important mechanical and thermodynamic parameters for describing the creep deformation mechanisms of solders [27]. In general, the deformation controlled by diffusion mechanism can be described by a power law equation [23]:

$$\dot{\varepsilon} = A\sigma^n \quad (1)$$

where $\dot{\varepsilon}$ is the strain rate, σ is the stress and A is the material-dependent constant.

Fig. 8 shows a linear relationship between UTS and strain rate (log–log plot), and the slope of each line (fitted to the experimental data) gives the so-called stress exponent, n. The n values at different temperatures for the tested alloys are listed in Table 3. The calculated n values at 25, 70 and 110 °C were; 5.7, 5.0 and 4.0 for SC, 8.0, 7.1 and 5.7 for SC–Ag, 6.1, 5.5 and 4.5 for SC–In and 9.8, 8.5 and 7.2, for SC–AgIn alloys, respectively. Incidentally, the quaternary alloy has the highest n values and the eutectic binary alloy SC has the lowest one, whereas the n values for the ternary alloys lying between these two alloy values at all testing temperatures. Besides, another phenomenon is that the apparent stress exponent n increases with decreasing temperature for all the Pb-free solders, which means that the precipitation-strengthening effect is greater at lower temperatures for all of the Pb-free alloys [28].

Table 3
Stress exponent (n) values for Sn–0.7Cu, Sn–0.7Cu–2Ag, Sn–0.7Cu–2In and Sn–0.7Cu–2Ag–2In solder alloys.

Alloy	Temperature (°C)	n
Sn–0.7Cu	25	5.7
	70	5.0
	110	4.0
Sn–0.7Cu–2Ag	25	8.0
	70	7.1
	110	5.7
Sn–0.7Cu–2In	25	6.1
	70	5.5
	110	4.5
Sn–0.7Cu–2Ag–2In	25	9.8
	70	8.5
	110	7.2

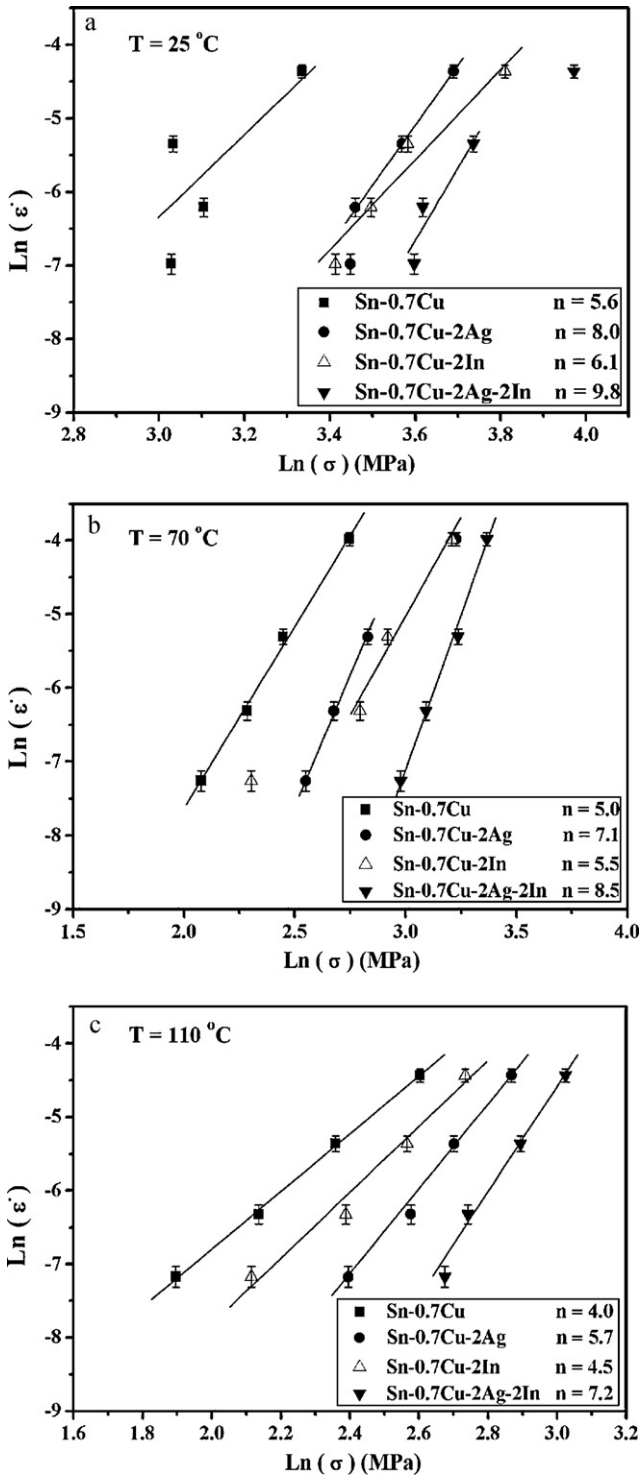

Fig. 8. Applied stress dependence on the steady-state creep strain rate for determination stress exponent (n) values at temperature (a) T = 25 °C, (b) T = 70 °C and (c) T = 110 °C for Sn–0.7Cu, Sn–0.7Cu–2Ag, Sn–0.7Cu–2In and Sn–0.7Cu–2Ag–2In solder alloys.

The stress exponent values have been frequently used to determine the mechanisms controlling the deformation process. However, it should be cautioned that making mere comparisons of the stress exponents, without additional information on activation energies, does not provide sufficient information to draw insightful comparisons on creep mechanisms of materials. At best, creep stress exponents can only help to narrow the field among

many theoretical possibilities [29]. In fact, deformation of polycrystalline materials at homologous temperatures above $0.5T_m$ can takes place by different deformation mechanisms, associated with different stress exponent values. A lot of multi-axial creep damage constitutive equations have been accounted to analyze the creep damage and failure of different materials [30–32,35].

In general, large n values have been observed in dispersion strengthened alloys. In Table 3, large n values obtained at low testing temperature, e.g. 25 and 70 °C, suggest that the dispersion precipitation strengthening is the more dominant in this temperature range. It is well known that precipitation strengthening can be sustained below $0.7T_m$. In addition, it is reported that diffusional creep is associated with n values around 1 and grain boundary sliding leads to n values close to 2 whereas the dislocation climb is responsible for n values in the range of 4–6 [33]. It has been shown by Edward and Ashby [26] that grain boundary sliding is an important cause for voids nucleation at grain boundaries. Grain boundary sliding can be accommodated in various ways: elastic accommodation, diffusion flow, or plastic flow. If the incompatibility caused by grain boundary sliding cannot be accommodated in any of these ways, voids will appear and grow at grain boundary. Accordingly, in the present investigation, the relatively high n values (7.2–9.8) imply that the operative creep mechanism in these alloys is the dislocation creep, similar to that of SAC solder [27]. On the other hand, the low n values of (4–6.1) is very close to that of pure Sn at 80–120 °C [34], implying that a creep deformation mechanism is dominated by dislocation climb mechanism.

4. Conclusions

Tensile tests for Sn–0.7Cu (SC), Sn–0.7Cu–2Ag (SC–Ag), Sn–Cu–2In (SC–In) and Sn–0.7Cu–2Ag–2In (SC–AgIn) solders were conducted. The effects of Ag and/or In additive, strain rate and temperature on the mechanical properties of the four solder alloys were investigated. The effects of Ag and/or In content on the microstructures of solder were also studied. Some important results and conclusions are summarized as follows:

1. The strain rate and temperature dependent mechanical property for the YS, UTS and elongation have been studied. Both UTS and YS decreased with increasing temperatures but they increased with increasing strain rate, whereas the ductility changes with inconsistent behaviors for the lead-free solders.
2. Sn–0.7Cu–2Ag–2In solder exhibited superior combination of mechanical properties (in terms of (YS (∼255%), UTS (∼215%) and ductility) when compared with the other commercially available Sn–0.7 wt. % Cu solder alloys.
3. The experimental stress exponent values of SC–AgIn alloy were higher than that of other studied alloys at all temperature range.
4. From microstructural analysis, some new IMCs phases are developed in β-Sn matrix compared with the Sn–0.7Cu eutectic solder alloy such as; Ag_3Sn in Sn–0.7Cu–2Ag solder, Ag_3Sn and γ-$InSn_4$ in Sn–0.7Cu–2In as well as Ag_3Sn, γ-$InSn_4$ and In_4Ag_9 in Sn–0.7Cu–2Ag–2In solder alloys. The presence of the second phases has been shown to trigger the microstructural mechanism that enhances the mechanical properties of Sn–0.7Cu eutectic solder alloy.

References

[1] C.P. Lin, C.M. Chen, Y.W. Yen, H.J. Wu, S.W. Chen, J. Alloys Compd. 509 (2011) 3509–3514.
[2] J. Keller, D. Baither, U. Wilke, G. Schmitz, Q. Yu, H.P. Xie, L. Wang, Acta Mater. 59 (2011) 2731–2741.
[3] A.A. El-Daly, A. Fawzy, A.Z. Mohamad, A.M. El-Taher, J. Alloys Compd. 509 (2011) 4574–4582.
[4] A.K. Gain, T. Fouzder, Y.C. Chan, A. Sharif, N.B. Wong, W.K.C. Yung, J. Alloys Compd. 506 (2010) 216–223.
[5] C.Y. Lin, U.S. Mohanty, J.H. Chou, J. Alloys Compd. 501 (2010) 204–210.
[6] A.K. Gain, T. Fouzder, Y.C. Chan, W.K.C. Yung, J. Alloys Compd. 509 (2011) 3319–3325.
[7] X. Li, F. Zhang, F. Zu, X. Lv, Z. Zhao, D. Yang, J. Alloys Compd. 505 (2010) 472–475.
[8] A.A. El-Daly, F. El-Tantawy, A.E. Hammad, M.S. Gaafar, E.H. El-Mossalamy, A.A. Al-Ghamdi, J. Alloys Compd. 509 (2011) 7238–7246.
[9] E. Hodulova, M. Pacut, E. Lechovic, B. Simekova, K. Ulrich, J. Alloys Compd. 509 (2011) 7052–7059.
[10] G. Zeng, S. Xue, L. Gao, L. Zhang, Y. Hu, Z. Lai, J. Alloys Compd. 509 (2011) 7152–7161.
[11] G. Li, Y. Shi, H. Hao, Z. Xia, Y. Lei, F. Guo, J. Alloys Compd. 491 (2010) 382–385.
[12] G. Zeng, S. Xue, L. Zhang, L. Gao, J. Mater. Sci.: Mater. Electron 22 (2011) 565–578.
[13] B.S.S. Chandra Rao, K.M. Kumar, V. Kripesh, K.Y. Zeng, Mater. Sci. Eng. A 528 (2011) 4166–4172.
[14] T. H. Chuang, M. W. Wu, S. Y. Chang, S. F. Ping, L. C. Tsao, J. Mater. Sci: Mater. Electron. doi:10.1007/s10854-010-0253-1.
[15] S.M. Joo, H.K. Kim, Mater. Sci. Eng. A 528 (2011) 2711–2717.
[16] T. Ventura, S. Terzi, M. Rappaz, A.K. Dahle, Acta Mater. (2011), doi:10.1016/j.actamat.2011.03.044.
[17] A.A. El-Daly, A.E. Hammad, Mater. Sci. Eng. A 527 (2010) 5212–5219.
[18] S. Wiese, K.J. Wolter, Microelectron. Reliab. 44 (2004) 1923–1931.
[19] C. Andersson, P. Sun, J. Liu, J. Alloys Compd. 457 (2008) 97–105.
[20] M.E. Alam, S.M.L. Nai, M. Gupta, J. Alloys Compd. 476 (2009) 199–206.
[21] F.X. Che, W.H. Zhu, E.S.W. Poh, X.W. Zhang, X.R. Zhang, J. Alloys Compd. 507 (2010) 215–224.
[22] F. Zhu, H. Zhang, R. Guan, S. Liu, Microelectron. Eng. 84 (2007) 144–150.
[23] Q.S. Zhu, Z.G. Wang, S.D. Wu, J.K. Shang, Mater. Sci. Eng. A 502 (2009) 153–158.
[24] A.A. El-Daly, Phys. Stat. Sol. A 201 (9) (2004) 2035–2041.
[25] A.F. Ashby, G.H. Edward, Acta Metall. 26 (1978) 1379–1388.
[26] G.H. Edward, M.F. Ashby, Acta Metall. 27 (1979) 1505–1518.
[27] Z. Liang, X. Song-bai, G. Li-li, Z. Guang, C. Yan, Y. Sheng-lin, S. Zhong, Trans. Nonferr. Met. Soc. Chin. 20 (2010) 412–417.
[28] M.L. Huang, C.M.L. Wu, L. Wang, J. Electron. Mater. 34 (2005) 1373–1377.
[29] R. Mahmudi, A.R. Geranmayeh, H. Khanbareh, N. Jahangiri, Mater. Des. 30 (2009) 574–580.
[30] A.C.F. Cocks, M.F. Ashby, Met. Sci. Heat Treat. 14 (1980) 395–402.
[31] A.C.F. Cocks, A.F. Ashby, Prog. Mater. Sci. 27 (1982) 189–244.
[32] A.C.F. Cocks, A.F. Ashby, Met. Sci. J. 16 (1982) 465–474.
[33] C.M.L. Wu, D.Q. Yu, C.M.T. Law, L. Wang, Mater. Sci. Eng. R 44 (2004) 1–44.
[34] I. Shohji, T. Yoshida, T. Takahashi, S. Hioki, Mater. Sci. Eng. A 366 (2004) 50–55.
[35] H.T. Yao, F.Z. Xuan, Z. Wang, S.T. Tu, Nucl. Eng. Des. 237 (2007) 1969–1986.